CHEMPHYSCHEM

Supporting Information

Meaning and Measurability of Single-Ion Activities, the Thermodynamic Foundations of pH, and the Gibbs Free Energy for the Transfer of Ions between Dissimilar Materials

Alan L. Rockwood*[a, b]

cphc_201500044_sm_miscellaneous_information.pdf

Contents

1. Additional Experimental Details

Syntheses of compounds and characterization. The details of the synthesis and purification of **F1**, **F2**, **F8** and **M** are described elsewhere.[S1-S2] For OPE backbone reference compound **B**, all solvents and reagents were purchased from commercial sources and used as received without further purification. Diisopropylamine (99%) was degassed by sparging argon gas for 30 min prior to application. 4,5-Di-*n*-hexyl-1,2-ethynylbenzene was synthesized according to the literature procedure.[S3] Column chromatography was performed using silica gel Si_{60} (0.035–0.070 mm). Recycling-gel permeations chromatography (GPC) was performed on a Shimadzu GPC system (LC-20AD prominence pump; SPD-MA20A prominence diode array detector) equipped with two preparative columns (JAIGEL 1H+2H) with $CHCl_3$ as eluent at a flow rate of 3.5 mL min^{-1} and a pressure of 20 MPa. ^1H and ^{13}C NMR spectra were recorded on Bruker Avance 400 and calibrated to the residual solvent peak. MALDI-TOF mass spectrum (MS) was recorded on an Autoflex II from Bruker Daltonics. High-resolution mass spectrum (ESI) was recorded on an ESI MicrOTOF Focus from Bruker Daltonics. For evaluating optical properties of **B**, steady-state absorption and fluorescence spectroscopic measurements were conducted with spectroscopic grade solvents (Uvasol®) from Merck (Hohenbrunn, Germany) by using conventional quartz cells (light path 1 cm). The UV/Vis spectrum was recorded on a Perkin-Elmer UV/Vis spectrometer Lambda 35 and a Perkin Elmer Peltier temperature controller was used. The fluorescence emission spectrum was recorded with a PTI QM-4/2003 spectrometer. Polarizers in the specified set-up applying magic angle conditions 54.7° were used. The fluorescence quantum yield was determined by optical dilution method ($OD_{max} < 0.05$) and was determined as the average value for five different excitation wavelengths using pyrene as reference compound (Φ_{fl} (cyclohexane) = 0.32).[S4]

Computational methods. In order to gain insight into the spatial alignments of the unit PBI chromophores in the folded and extended conformations of **F8**, we performed geometry optimizations with a dispersion-corrected DFT-D approach (B97D)[S5] and cost-efficient STO-3G[S6] basis sets in Gaussian 09 (Gaussian, Inc.)[S7] for the simplest subunit of **F8**, *i.e*. for the folded and unfolded conformations of **F2**. The starting structures for the DFT-D calculations were the energy-minimized structures obtained with the force fields MM3* in MacroModel 9.8 within Maestro 9.3 (Schrödinger, LLC)[S8] and OPLS-AA in Tinker 6.2 (Jay W. Ponder Lab).[S9] With these methods the folded and unfolded conformations of **F2** could be realized, which satisfyingly mimic our systems in $CHCl_3$ and THF/MCH, respectively. Nevertheless, in the case of **F8**, which owns a much larger structure than its model compound **F2**, DFT calculations

become too expensive and time-consuming and we adopted the results[S2] obtained by applying AMBER force-field in HyperChem[S10] for both folded and unfolded structures of **F8**.

In our previous report on the reference compound **F2**[S1] we state that the backbone appears to be significantly distorted out of plane in order to achieve the conformation with the lowest energy (*ca*. 4 kJ/mol lower in energy than the non-distorted form). Since the reorientation of the OPE moiety has no tremendous effect on the overall energy or the 3-dimensional arrangement of the dye systems, we assume that such reordering takes place more likely for small representatives of our system. On the other hand, for the larger **F8** system, the scaffold is enlarged and thus more ponderous, so that such events are more unlikely and can be neglected in the discussion of our results. Therefore, we are convinced that the structural information deduced by force-field calculations is sufficient to represent the spatial arrangement of **F8**.

2. Supporting Information

Synthesis of 4,5-di-*n*-hexyl-1,2-(phenylethynylene)benzene (OPE backbone B).

In a 50 mL flask were placed 66.2 mg (225 µmol) 4,5-di-*n*-hexyl-1,2-ethynylbenzene, 4.8 mg (25.2 µmol) copper(I) iodide, and 5.5 mg (7.84 µmol) bis(triphenylphosphino)palladium(II) dichloride under nitrogen atmosphere. The flask was evacuated again and 10 mL degassed diisopropylamine were added under nitrogen atmosphere. A second solution containing 103 mg (504 µmol) iodobenzene in 4 mL diisopropylamine was prepared under nitrogen. Both flasks were degassed by two "freeze-pump-thaw" cycles to remove residual oxygen. The solution containing iodobenzene was then collected by a syringe and dropped into the first solution with a septum at 50 °C within 30 min. The reaction mixture was stirred over night at 50 °C. After being cooled to room temperature, the reaction mixture was poured into a 2 M aqueous hydrogen chloride solution, diluted with *n*-hexane and washed with water. The combined organic layers were dried over magnesium sulfate and the solvent was removed by a rotary evaporator. The resulting crude product was purified by column chromatography on silica gel (*n*-hexane/dichloromethane, 3/1 (v/v)) to obtain pre-purified compound. As other reaction by-products could not be separated from the product, recycling GPC was used to get pure compound in the form of yellow viscous oil (19.9 mg, 44.6 µmol; 20%).

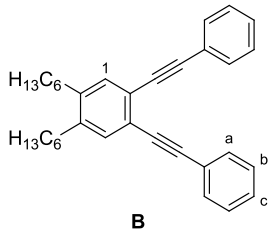

B

^{1}H NMR (400 MHz, 300 K, CD_2Cl_2): δ = 7.59–7.55 (m, 4H, H_a), 7.40–7.34 (m, 8H, $H_{1,b,c}$), 2.63 (t, ^{3}J = 7.90 Hz, 4H, CCH_2), 1.65–1.57 (m, 4H, CCH_2CH_2), 1.43–1.33 (m, 12H, CH_2), 0.92 ppm (t, ^{3}J = 7.13 Hz, 6H, $(CH_2)_5CH_3$).

^{13}C NMR (101 MHz, 300 K, CD_2Cl_2): δ = 142.1, 132.8, 131.9, 128.9, 128.7, 123.9, 123.2, 92.7, 89.0, 32.9, 32.2, 31.3, 29.8, 23.0, 14.3 ppm.

MS (MALDI, matrix: DCTB; positive, chloroform): calcd. for $C_{34}H_{38}$ $[M]^+$ 446.297, found 446.208.

HRMS (ESI, positive, acetonitrile/chloroform = 1/1): calcd. for $C_{34}H_{39}$ $[M+H]^+$ 447.30518, found 447.30432.

UV/Vis (CH_2Cl_2): λ_{max} (ε) = 266 (39600), 281 (67000), 317 nm (21600 M^{-1} cm^{-1}).

Fluorescence (CH_2Cl_2): λ_{max} = 368 nm (λ_{ex} = 320 nm); Φ_{fl} = 0.30.

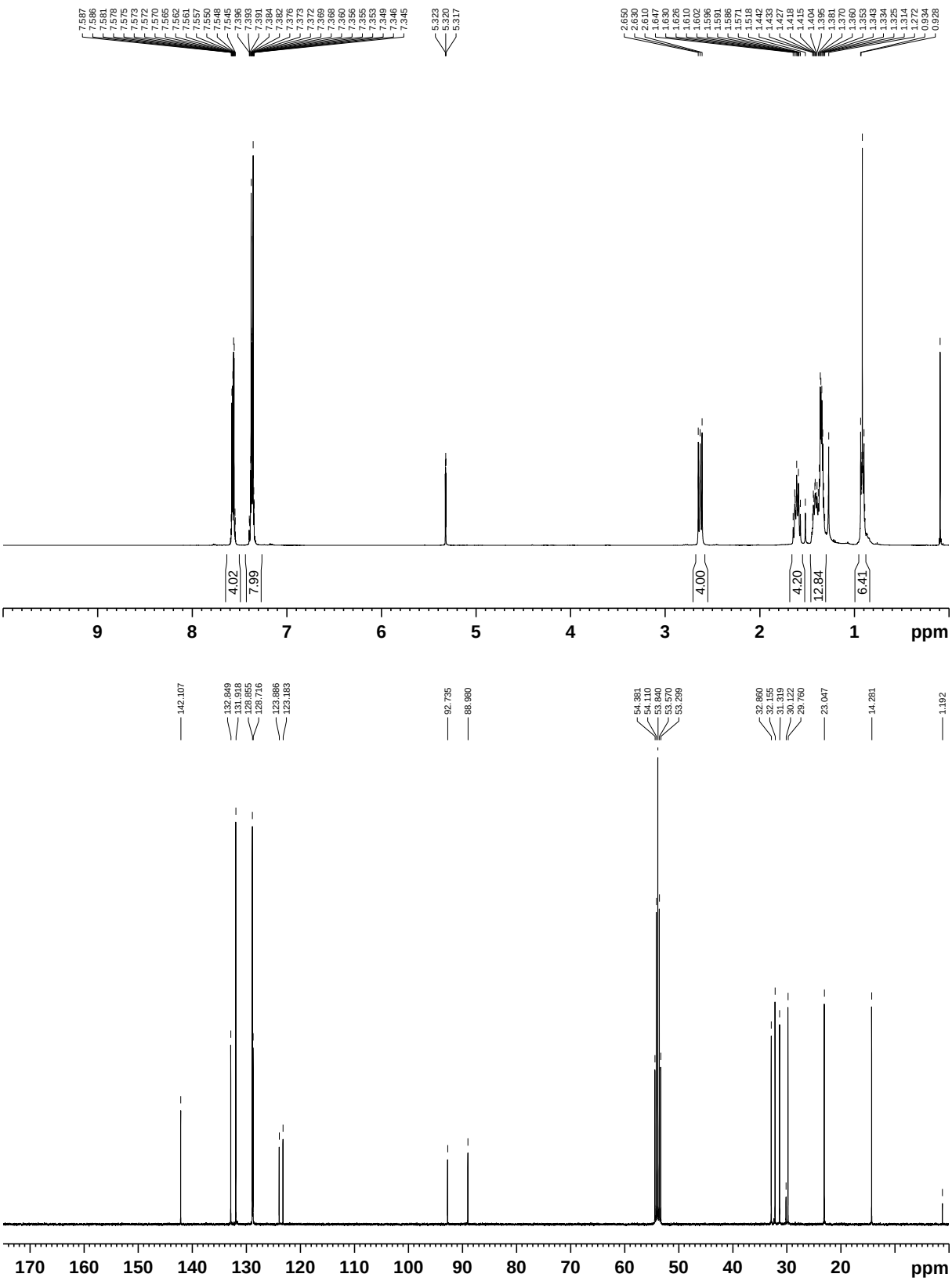

^{1}H NMR (400 MHz, top) and ^{13}C NMR spectra (101 MHz, bottom) of **B** in CD_2Cl_2 at 300 K.

Details of the Förster-type energy transfer analysis for the extended form of F8.

The extended structure of **F8**, which maintains a sufficiently large distance between the PBI units (16.3 Å), can be treated with the point-dipole approximation, and the EET rates can also be mechanistically estimated by the Förster-type incoherent energy hopping model[S11] (Equation (S1)):

$$k_{EET}(r) = \frac{Q_D \kappa^2}{\tau_D r^6}\left(\frac{9000(\ln 10)}{128\pi^5 N_A n^4}\right)\int_0^\infty F_D(\lambda)\varepsilon_A(\lambda)\lambda^4 d\lambda \quad \text{(S1)}$$

(Q_D: quantum yield of the donor, κ^2: orientation factor between the transition dipole moments of the donor and the acceptor, τ_D: fluorescence lifetime of the donor, r: donor-acceptor distance, ε_A: extinction coefficient of the acceptor at λ in $M^{-1}cm^{-1}$, N_A: Avogadro's number, n: refractive index of the medium, $F_D(\lambda)$: fluorescence intensity)
where the spectral overlap between the donor emission and the acceptor absorption J is defined in Equation (S2):

$$J = \int_0^\infty F_D(\lambda)\varepsilon_A(\lambda)\lambda^4 d\lambda \quad \text{(S2)}$$

In our system, we assume that only the homotransfer between identical PBI monomer units occurs, *i.e*. a PBI monomer (**M**; see Figure S5) serves as both the donor and the acceptor. Individual parameters used for the calculation of k_{EET} are as follows:

Q_D = 0.89
τ_D = 3.9 ns (see Figure S5 for the fluorescence decay profile)
r = 16.3 Å (the averaged center-to-center distances between adjacent PBI units; see Table S2 for individual parameters)
n = 1.446 (refractive index of $CHCl_3$ at 20 °C)
$J = 2.26\times10^{15}$ $M^{-1}cm^{-1}nm^4$
κ^2 = 1.96

The orientation factor κ^2 was calculated according to Equation (S3)

$$\kappa^2 = (\cos\varphi - 3\cos\theta_A\cos\theta_B)^2 \quad \text{(S3)}$$

where φ, θ_A and θ_B represent the angles indicated below (μ_A, μ_B represent the transition dipole vector of each donor and acceptor unit and r is the center-to-center distance).

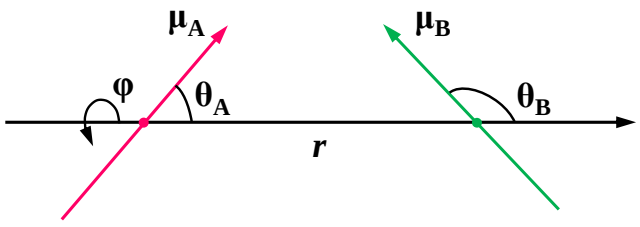

φ = 117.2°
θ_A = 43.4°, θ_B = 148.5° (All values are taken from the averaged angle values between adjacent PBI units)

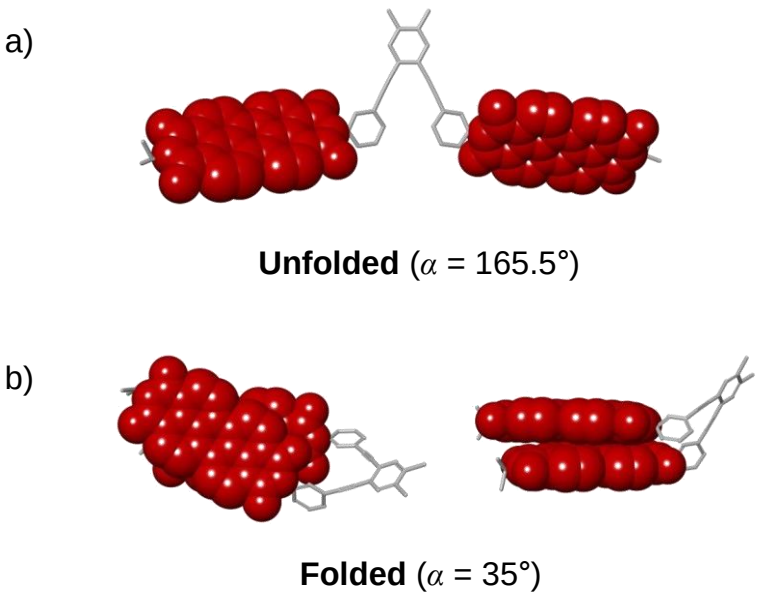

Figure S1. Schematic drawings of the DFT-D geometry-optimized (B97D/STO-3G) structures of **F2** in a) unfolded and b) folded (left: top view; right: side view) form, respectively (*α*: azimuth angle between the in-plane polarized transition dipole moments of the two PBI units assumed to be stacked perpendicular to the helix axis).

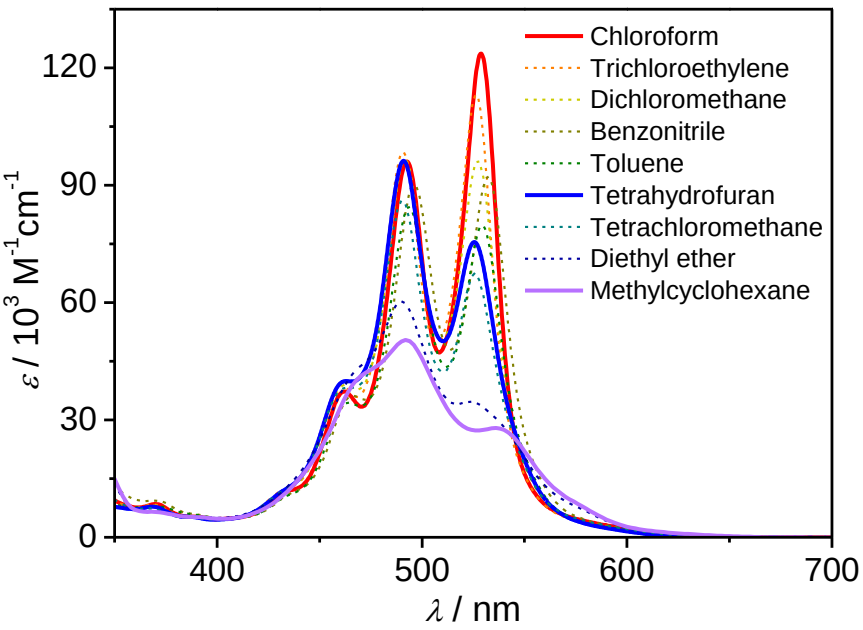

Figure S2. Steady-state absorption spectra of **F2** in nine different organic solvents.

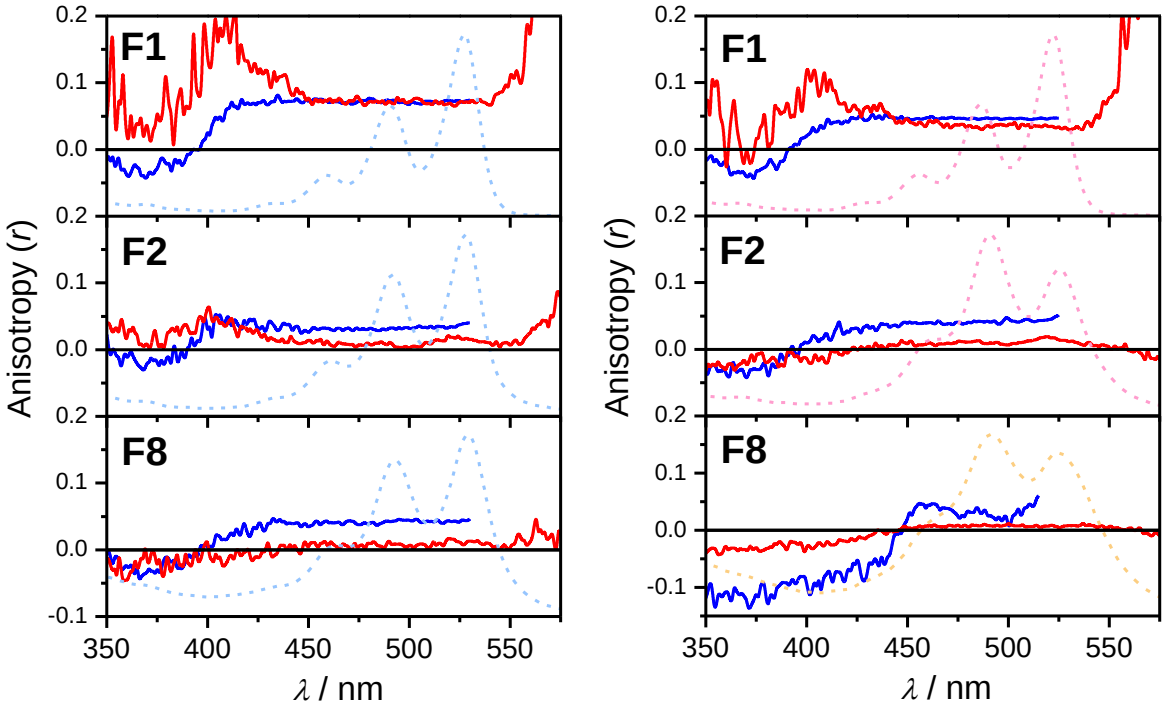

Figure S3. Steady-state fluorescence excitation anisotropy spectra at the emission wavelengths of 540 nm (blue) and 625 nm (red), respectively, and excitation spectra (dashed lines) of **F1**, **F2** and **F8** in $CHCl_3$ (left column) and of **F1** and **F2** in THF as well as **F8** in MCH (right column).

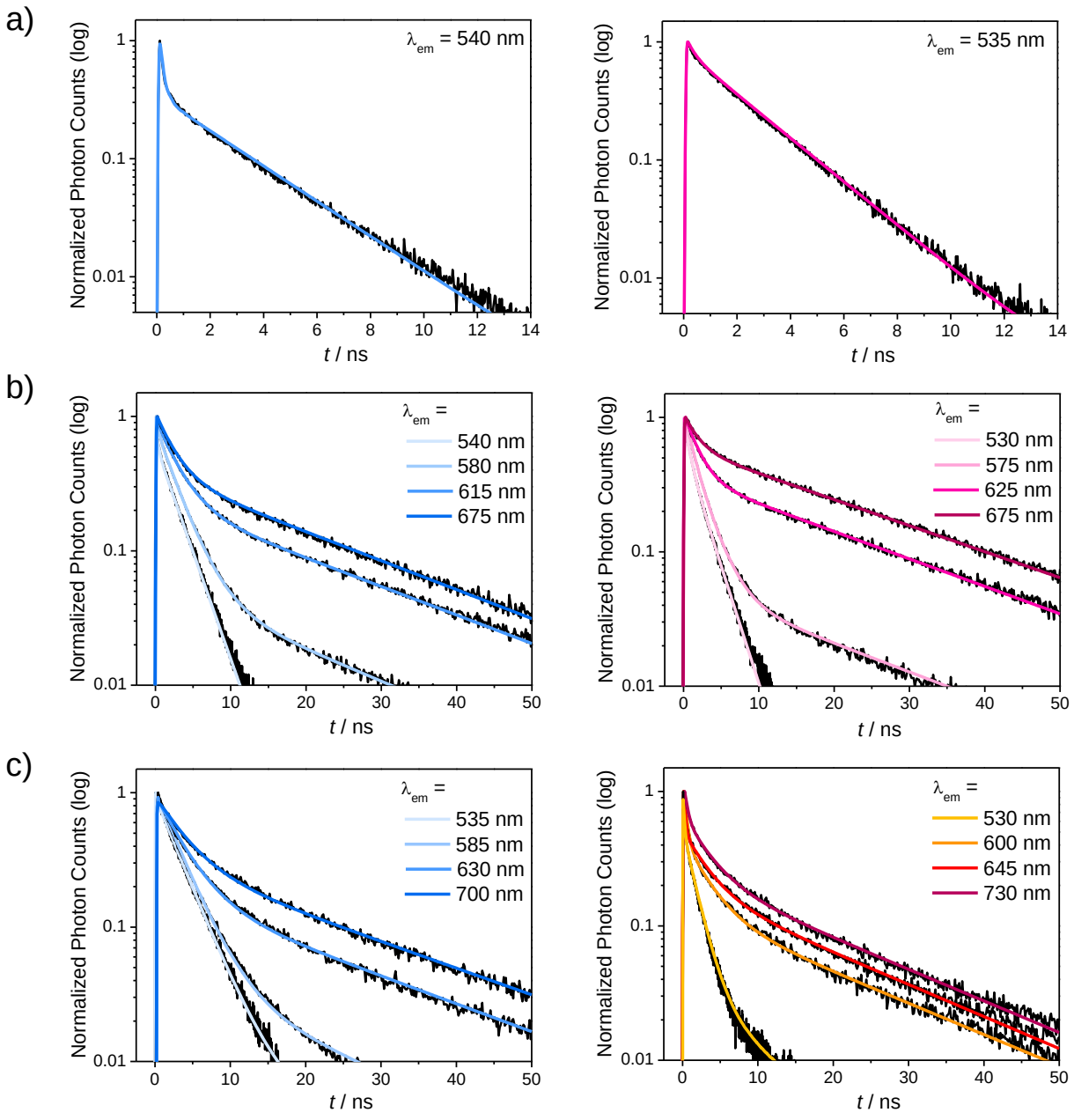

Figure S4. Fluorescence decay profiles of a) **F1**, b) **F2** and c) **F8** in $CHCl_3$ (blue fitted lines), THF (rosa-magenta fitted lines) and MCH (orange-red fitted lines) by employing the excitation wavelength of 450 nm. The monitored emission wavelengths are indicated in each figure.

Table S1. Fitted decay parameters of emission wavelength dependent fluorescence decay profiles of **F1**, **F2** and **F8** in different solvents.

Cmpd.	Solvent	λ_{em}[a] (nm)	τ_1[c,d] (ns)	τ_2[c] (ns)	τ_3[c] (ns)
F1	$CHCl_3$	540[b]	< 0.05 (81)	2.7 (19)	-
	THF	540[b]	< 0.05 (36)	2.3 (64)	-
F2	$CHCl_3$	540	< 0.05 (62)	2.7 (38)	-
		580	-	2.7 (94)	20.0 (6)
		625	-	2.7 (75)	20.0 (25)
		675	-	2.7 (67)	20.0 (33)
	THF	530	< 0.05 (37)	2.0 (63)	-
		575	-	2.0 (94)	20.0 (6)
		625	-	2.0 (68)	20.0 (32)
		675	-	2.0 (45)	20.0 (55)
F8	$CHCl_3$	535	< 0.05 (30)	3.0 (70)	-
		585	-	3.0 (95)	20.1 (5)
		630	-	3.0 (80)	20.1 (20)
		700	-	3.0 (66)	20.1 (34)
	MCH	530	< 0.05 (39)	3.0 (58)	19.5 (3)
		600	-	3.0 (78)	19.5 (22)
		645	-	3.0 (67)	19.5 (33)
		730	-	3.0 (55)	19.5 (45)

[a] Monitored emission wavelength. [b] **F1** did not show any wavelength dependence and therefore only the results at 540 nm are presented here. [c] The values in the parentheses represent the normalized pre-exponential factors. [d] The accurate timescales of the short components could not be determined due to the instrumental response (~50 ps) of our setup.

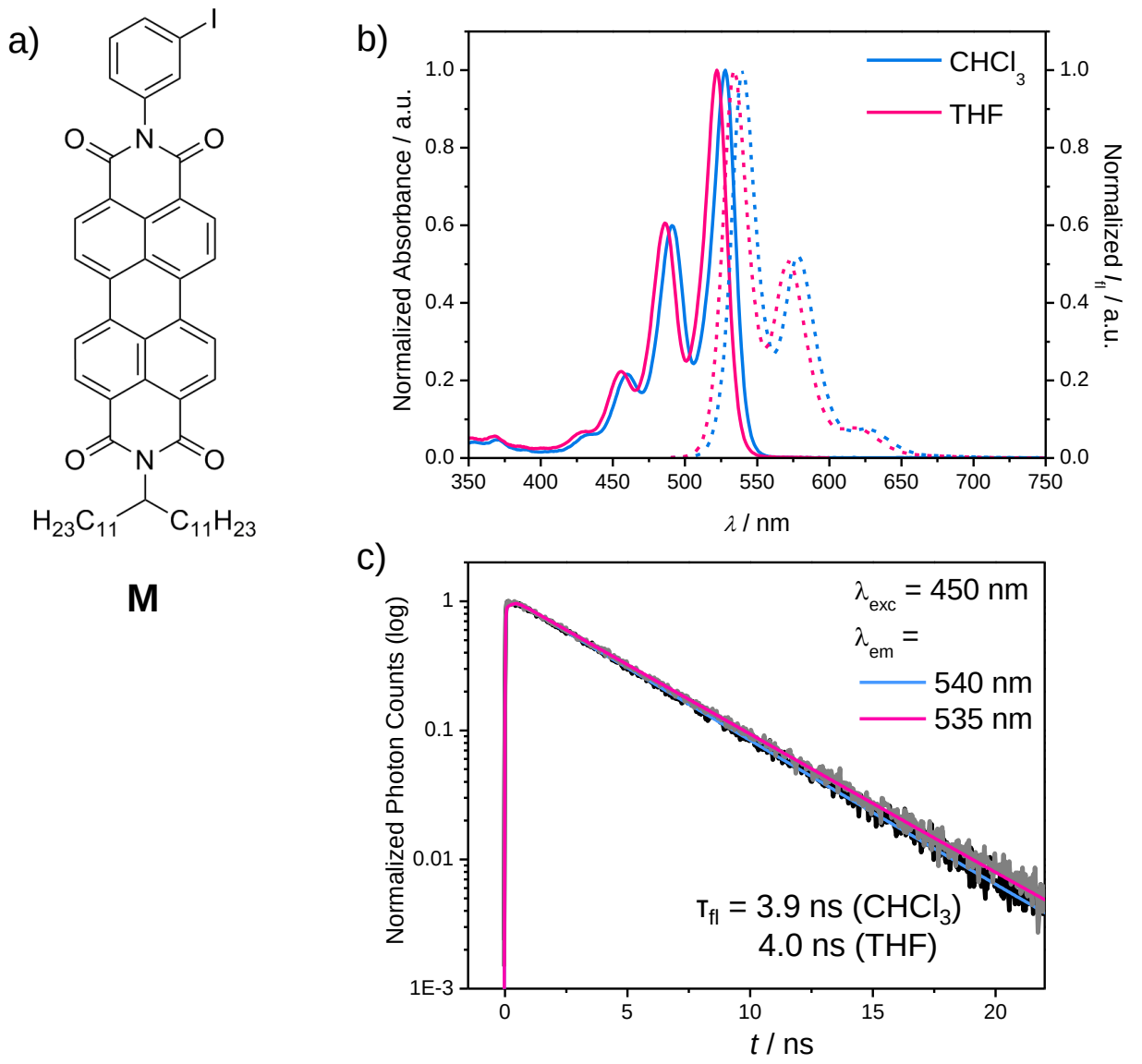

Figure S5. a) Molecular structure of the backbone-free monomer **M**. b) Steady-state absorption (solid lines) and fluorescence emission (dashed lines) spectra of **M** in $CHCl_3$ (blue) and THF (magenta). The excitation wavelength used for the fluorescence measurement is 480 nm. c) Fluorescence decay profiles of **M** in $CHCl_3$ (blue fitted line) and THF (magenta fitted line) by employing the excitation wavelength of 450 nm and emission wavelength of 540 and 535 nm, respectively. The fitted parameters are indicated inside the figure.

*Note: Measurements in MCH were not possible due to very low solubility of **M** in MCH.

a)

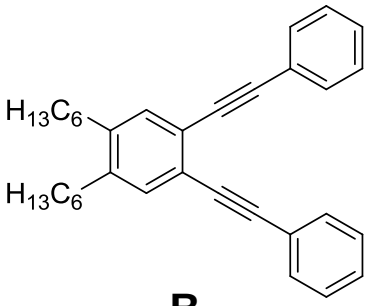

B

b)

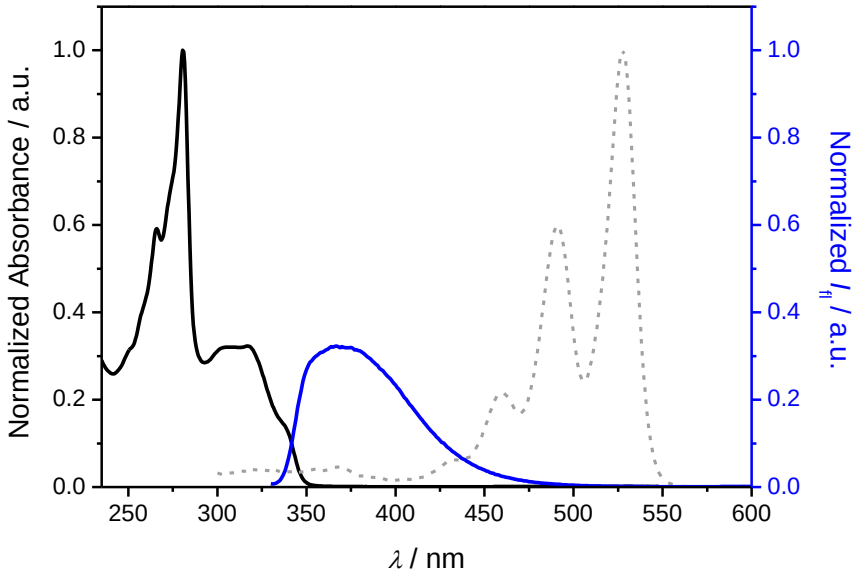

Figure S6. a) Molecular structure and b) steady-state absorption (black) and fluorescence emission (blue) spectra of backbone **B** in dichloromethane. The excitation wavelength employed for the fluorescence measurement is 320 nm. The gray dotted trace shows the steady-state absorption spectrum of **M** in $CHCl_3$.

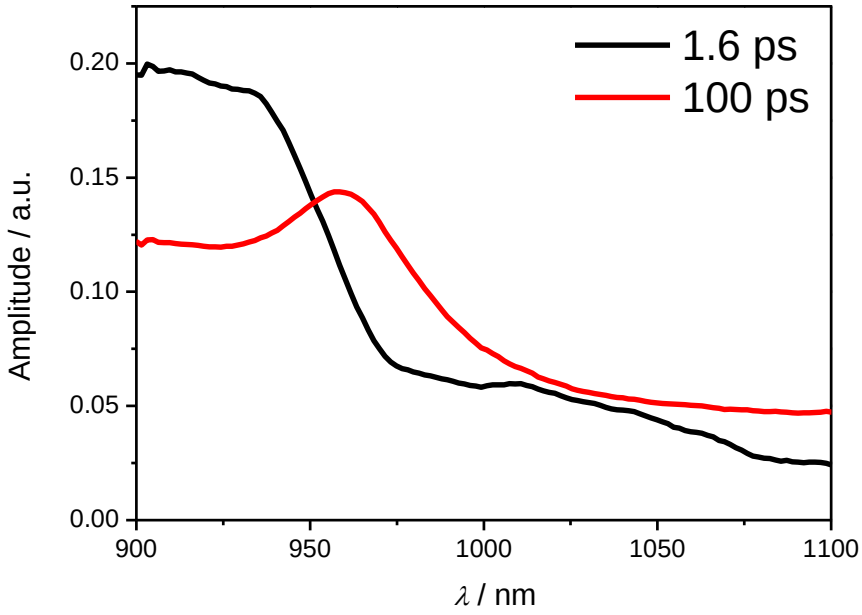

Figure S7. Decay associated spectra (DAS) obtained from global analysis of the TA spectra of **F8** in $CHCl_3$ at NIR probe. The fitted decay parameters of each principal component are indicated inside the figure.

Table S2. Center-to-center distances and azimuth angles (α) between neighboring PBI units in the unfolded and folded structure of **F8**, respectively, obtained by AMBER force-field optimization. The numbering of the eight PBI units is illustrated below.

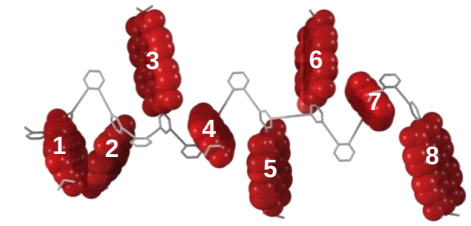

Structure		Parameters							
		1 - 2	2 - 3	3 - 4	4 - 5	5 - 6	6 - 7	7 - 8	Average
Unfolded	Center-to-Center Distance (Å)	16.4	15.7	16.1	16.1	16.4	16.3	16.9	16.3
	Azimuth Angle (°)	132.5	118.0	117.5	113.0	107.0	112.5	120.0	117.2
Folded	Center-to-Center Distance (Å)	3.35	3.35	3.38	3.48	3.38	3.34	3.41	3.38
	Azimuth Angle (°)	49.5	47.0	45.5	52.0	48.5	47.0	46.0	47.9

3. References

[S1] B. Fimmel, M. Son, Y. M. Sung, M. Grüne, B. Engels, D. Kim, F. Würthner, *Chem. Eur. J.* **2015**, *21*, 615-630.

[S2] V. Dehm, M. Büchner, J. Seibt, V. Engel, F. Würthner, *Chem. Sci*. **2011**, *2*, 2094-2100.

[S3] Q. Zhou, P. Carroll, T. M. Swager, *J. Org. Chem.* **1994**, *59*, 1294-1301.

[S4] I. B. Berlman, *Handbook of Fluorescence Spectra of Aromatic Molecules*, 2nd ed., Academic Press, New York, London, **1971**.

[S5] S. Grimme, *J. Comp. Chem.* **2006**, *27*, 1787-1799.

[S6] a) W. J. Hehre, R. F. Stewart, J. A. Pople, *J. Chem. Phys.* **1969**, *51*, 2657-2664; b) J. B. Collins, P. v. R. Schleyer, J. S. Binkley, J. A. Pople, *J. Chem. Phys.* **1976**, *64*, 5142-5152.

[S7] M. J. Frisch, G. W. T., H. B. Schlegel, G. E. Scuseria, M. A. Robb, J. R. Cheeseman, G. Scalmani, V. Barone, B. Mennucci, G. A. Petersson, H. Nakatsuji, M. Caricato, X. Li, H. P. Hratchian, A. F. Izmaylov, J. Bloino, G. Zheng, J. L. Sonnenberg, M. Hada, M. Ehara, K. Toyota, R. Fukuda, J. Hasegawa, M. Ishida, T. Nakajima, Y. Honda, O. Kitao, H. Nakai, T. Vreven, J. A. Montgomery, Jr., J. E. Peralta, F. Ogliaro, M. Bearpark, J. J. Heyd, E. Brothers, K. N. Kudin, V. N. Staroverov, T. Keith, R. Kobayashi, J. Normand, K. Raghavachari, A. Rendell, J. C. Burant, S. S. Iyengar, J. Tomasi, M. Cossi, N. Rega, J. M. Millam, M. Klene, J. E. Knox, J. B. Cross, V. Bakken, C. Adamo, J. Jaramillo, R. Gomperts, R. E. Stratmann, O. Yazyev, A. J. Austin, R. Cammi, C. Pomelli, J. W. Ochterski, R. L. Martin, K. Morokuma, V. G. Zakrzewski, G. A. Voth, P. Salvador, J. J. Dannenberg, S. Dapprich, A. D. Daniels, O. Farkas, J. B. Foresman, J. V. Ortiz, J. Cioslowski, D. J. Fox, Gaussian 09, Revision B.01; Gaussian, Inc.: Wallingford, CT, 2010.

[S8] a) Maestro, version 9.3, Schrödinger, LLC, New York, NY, 2011; b) MacroModel, version 9.8, Schrödinger, LLC, New York, NY, 2011.

[S9] J. W. Ponder, *Tinker*, version 6.2; Jay W. Ponder Lab: Saint Louis, MO, 2013.

[S10] HyperChem, Release 7.1 for Windows, Hypercube, Inc., Gainesville, FL, 2002.

[S11] J. R. Lakowicz, *Principles of Fluorescence Spectroscopy*, 2nd ed., Kluwer Academic/Plenum Publishers, New York, Boston, Dordrecht, London, Moscow, **1999**.